Nanoscale

PAPER

Check for updates

Cite this: *Nanoscale*, 2020, **12**, 20859

Preserving the shape of silver nanocubes under corrosive environment by covering their edges and corners with iridium†

Peng Wang,[a,b] Jaewan Ahn,[a] Ruoqi Gao[a] and Dong Qin *[a]

Silver nanocubes have found use in an array of applications but their performance has been plagued by the shape instability arising from the oxidation and dissolution of Ag atoms from the edges and corners. Here we demonstrate that the shape of Ag nanocubes can be well preserved by covering their edges and corners with a corrosion-resistant metal such as Ir. In a typical process, we titrate a Na_3IrCl_6 solution in ethylene glycol (EG) into a suspension of Ag nanocubes in an EG solution in the presence of poly(vinylpyrrolidone) (PVP) held at 110 °C. The Ir atoms derived from the reduction of Na_3IrCl_6 by EG and Ag are deposited onto the edges and then corners for the generation of Ag–Ir core-frame nanocubes. Remarkably, our results indicate that a small amount of Ir atoms on the edges and corners is adequate to prevent the Ag nanocubes from transforming into nanospheres when heated in a PVP/EG solution up to 110 °C. We further demonstrate that these Ag–Ir nanocubes embrace plasmonic properties comparable to those of the original Ag nanocubes, making them immediately useful in a variety of applications. This strategy for stabilizing the shape of Ag nanocubes should be extendible to Ag nanocrystals with other shapes or nanocrystals comprised of other metals.

Received 14th August 2020,
Accepted 2nd October 2020

DOI: 10.1039/d0nr05969b

rsc.li/nanoscale

Introduction

Noble-metal nanocrystals are of critical importance to an array of fundamental studies and a broad spectrum of applications in photonics, catalysis, energy harvesting/conversion, sensing, and imaging.[1–5] It has been established that the properties of these nanocrystals and their merits in various applications depend on a set of parameters, including size, shape, elemental composition, and internal structure.[6–8] Among these parameters, shape has received the greatest interest in recent years owing to its strong correlations with the properties of a nanocrystal.[9,10] For example, the shape of a Ag nanocrystal defines its symmetry and thereby the number of modes allowed for localized surface plasmon resonance (LSPR),[11,12] as well as the presence of sharp corners and thus distribution of local electric fields essential to surface-enhanced Raman scattering (SERS).[13,14] On the other hand, the shape of a nanocrystal determines the fractions of atoms located at the corners, edges, and faces, in addition to the proportions of different types of facets exposed on the surface.[15] All of these factors are imperative in optimizing the activity and selectivity of a catalyst based on noble-metal nanocrystals.[16,17] For example, it was reported that the catalytic selectivity of Ag nanocubes toward ethylene epoxidation could be increased to 85%, much higher than the value of 40% for the conventional Ag nanoparticles featuring poorly defined shapes.[18]

Over the past decades, many groups have synthesized noble-metal nanocrystals with a variety of different shapes, including cubes, octahedra, tetrahedra, cuboctahedra, decahedra, icosahedra, bipyramids, plates or prisms, rods, wires, and concave cubes.[19–21] It is well-established that the shape taken by nanocrystals in a solution phase can be controlled by introducing different types of capping agents.[22,23] It is generally accepted that a capping agent can selectively bind to a facet to reduce its specific surface energy and thereby promote a growth pathway toward a maximum expression of this facet on the surface. This concept was well demonstrated using the synthesis of Ag nanocubes in ethylene glycol (EG), with poly(vinylpyrrolidone) (PVP) serving as a capping agent.[24] Because PVP selectively binds to the {100} facets of nanocrystals, the specific

[a]*School of Materials Science and Engineering, Georgia Institute of Technology, Atlanta, Georgia 30332, USA. E-mail: dong.qin@mse.gatech.edu*
[b]*School of Materials Science and Engineering, Shandong University of Technology, Zibo, Shandong 255000, P. R. China*

†Electronic supplementary information (ESI) available: Additional materials, experimental methods, TEM image of Ag nanocubes, UV–vis spectra recorded from suspensions of the Ag nanocubes before and after they had been treated in a PVP/EG solution at 110 °C for different periods of time and TEM images of the resultant nanoparticles, a schematic illustration of a Ag nanocube labelled with dimension, SERS spectra recorded from an aqueous suspension of the 2,6-DMPI-functionalized Ag–Ir nanocubes with laser excitation at 532 nm, SERS spectra recorded from an aqueous suspension of the 2,6-DMPI-functionalized Ag–Ir nanocubes after background subtraction and the corresponding curve fitting results, a table of ICP-MS results, calculation of the number of Ag nanocubes in the reaction, calculation of Ir atoms deposited onto a Ag nanocube, calculation of the surface coverage of Ir atoms on the edges and corners of a Ag nanocube. See DOI: 10.1039/d0nr05969b

This journal is © The Royal Society of Chemistry 2020

surface energies of low-index facets increase in the order of $\gamma_{\{100\}} < \gamma_{\{111\}} < \gamma_{\{110\}}$, leading to the formation of nanocubes enclosed by {100} facets.[25–27] While new, complex shapes have been demonstrated through the development of advanced protocols, it remains challenging to preserve the shape of a nanocrystal bearing sharp features for stabilizing its surface structure and related properties.[28–30] Taking Ag nanocubes as a typical example, they are highly vulnerable to degradation at an elevated temperature or in an oxidative environment, leading to the truncation at corners and edges toward the formation of particles enclosed by a mix of {111} and {100} facets. Such a change in shape tends to deteriorate their performance in SERS detection,[31] as well as their catalytic selectivity toward the epoxidation reaction.[18,32] It is not an overstatement that there is an ever-increasing gap between the ability to synthesize noble-metal nanocrystals with complex, diverse shapes and the competence to preserve the shapes.

When surface atoms are situated on different types of facets, they will differ in reactivity owing to the variations in surface energy.[33] As a general rule, atoms with the highest surface energy are most susceptible to oxidation and dissolution, contributing to the shape instability of a noble-metal nanocrystal.[34,35] In principle, one can suppress the shape instability of a nanocrystal by passivating those vulnerable sites with a metal lower in reactivity. Herein, we report a strategy for preserving the shape of Ag nanocubes in a PVP/EG solution heated to 110 °C in air by covering their edges and corners with Ir atoms. The choice of Ir is justified by the following arguments. Firstly, Ir is the most corrosion-resistant metal. For example, based on the potential-pH equilibrium diagram of the Ir–water system, it can remain intact in an aqueous solution at all pH values.[36] Secondly, Ir has a much higher melting point than that of Ag (2466 *vs.* 962 °C).[37] Thirdly, Ir inherits an fcc structure but there is 6% lattice mismatch between Ag and Ir, making it immiscible with Ag for excluding the formation of Ag–Ir alloy.[38] In a typical process, we disperse Ag nanocubes in a PVP/EG solution at 110 °C, followed by the titration of a Na_3IrCl_6/EG solution using a syringe pump. We demonstrate that the Ir atoms derived from the reduction of Na_3IrCl_6 are deposited on the edges and then corners of the Ag nanocubes for the generation of Ag–Ir core-frame nanocubes. By covering the edges and corners with Ir atoms, the resultant nanocrystals exhibit excellent shape stability when aged at 110 °C in a PVP/EG solution. In comparison, the pristine Ag nanocubes are transformed into nanospheres under the same condition. We further demonstrate that the AgIr nanocubes embrace plasmonic properties comparable to those of the original Ag nanocubes.

Experimental

Chemicals and materials

Ethylene glycol (EG) was acquired from J. T. Baker. Silver trifluoroacetate (CF_3COOAg, 99.99%), poly(vinylpyrrolidone) with an average molecular weight of 55 000 (PVP-55), sodium hydrosulfide hydrate ($NaHS{\cdot}xH_2O$), aqueous hydrochloric acid (HCl, 37% by weight), sodium hexachloroiridate(III) hydrate ($Na_3IrCl_6{\cdot}xH_2O$), 2,6-dimethylphenyl isocyanide (2,6-DMPI, ≥98.0%), and ethanol (200 proof) were all ordered from Sigma-Aldrich. Acetone (HPLC grade, ≥99.5%) was obtained from Alfa Aesar. Deionized (DI) water with a resistivity of 18.2 MΩ cm under ambient condition was used throughout the experiments.

Synthesis of Ag nanocubes

We followed a published protocol to prepare the Ag nanocubes with an average edge length of 38.7 ± 2.6 nm.[39] We washed the Ag nanocubes with acetone and water, once each, and then re-dispersed them in water at a concentration of 3.86 mg mL^{-1} for further use.

Evaluating the shape stability of Ag nanocubes

In a typical process, 0.05 g PVP was dissolved in 3.5 mL of EG hosted in a 23 mL glass vial. After heating at 110 °C under magnetic stirring at 360 rpm for 10 min, we injected 32 μL of the aqueous suspension of Ag nanocubes. We then withdrew 500 μL samples from the mixture at different time points of 1, 5, 10, 30 min, respectively, and quenched them in an ice-water bath. The solid products were washed with acetone at 6500 rpm for 15 min and then water at 14 000 rpm for 10 min. Finally, the solids were re-dispersed in water for characterization.

Synthesis of Ag–Ir nanocubes

In a standard procedure, 0.05 g PVP was dissolved in 3.5 mL of EG hosted in a 23 mL glass vial. After heating at 110 °C under magnetic stirring at 360 rpm for 10 min, we injected 32 μL of the aqueous suspension of Ag nanocubes, immediately followed by the titration of a Na_3IrCl_6 solution in EG (2 mM) at a rate of 4 mL h^{-1} using a syringe pump. After completion of titration, we allowed the reaction to proceed for 10 min before it was quenched in an ice-water bath. After the solid products had been washed with acetone at 6500 rpm for 15 min and then water at 14 000 rpm for 10 min, they were re-dispersed in 350 μL of water for further use.

Evaluating the shape stability of Ag–Ir nanocubes

The as prepared Ag–Ir nanocubes were centrifuged again at 14 000 rpm for 10 min, followed by re-dispersion in 40 μL of water. We followed the same procedure as decribed above for evaluating the stability of Ag nanocubes except that 32 μL of the Ag nanocubes were replaced by 33.5 μL of the Ag–Ir nanocubes.

SERS characterization of the Ag and Ag–Ir nanocubes

Initially, 100 μL of the as-prepared Ag–Ir nanocubes were dispersed in 1 mL of 2,6-DMPI ethanol solution (10^{-4} M) and allowed to rest at room temperature for 1 h. The 2,6-DMPI functionalized nanocubes were collected by centrifugation and washed with water twice before re-dispersion in 100 μL of

 This journal is © The Royal Society of Chemistry 2020

water. We used the same procedure to functionalize 9.14 μL of the Ag nanocubes to ensure that the number of Ag nanocubes was on the same order as that of the Ag–Ir nanocubes. In a typical SERS measurement, about 25 μL of the functionalized nanoparticles was added into a hole punched in a polydimethylsiloxane (PDMS) block, followed by the collection of Raman spectra under the excitation of a 532 nm laser, together with a 100× objective lens at 50 mW laser power and 10 s of collection time.

Quantitative analysis of the Raman data

We used Renishaw's WiRE 5.1 software to run the curve fitting for the ν_{NC} band of 2,6-DMPI present in the SERS spectra. For each data point, we loaded the raw data into the software and then centered the viewing window around the peak of interest (1800–2400 cm^{-1} for the ν_{NC} band). By using the curve-fitting function in the software, we fitted the data using a single or multiple Gaussian–Lorentzian peak(s). The software optimized the curve fit model to minimize the sum of the squared deviations of the fitting from the experimental data. For the SERS spectra recorded from aqueous suspensions of the 2,6-DMPI-functionalized Ag nanocubes, we used one Gaussian–Lorentzian peak to perform the optimization. For the SERS spectra recorded from aqueous suspensions of the 2,6-DMPI-functionalized Ag–Ir nanocubes prepared with 0.02 mL of Na_3IrCl_6 solution, we used one Gaussian–Lorentzian peak with its position fixed at 2169 cm^{-1} and another peak to perform the analysis, from which we obtained the position of another peak at 2117 cm^{-1}. For the SERS spectra recorded from aqueous suspensions of the 2,6-DMPI-functionalized Ag–Ir nanocubes prepared with 0.05 mL of Na_3IrCl_6 solution, we used two Gaussian–Lorentzian peaks with their positions fixed at 2169 and 2117 cm^{-1}, and another one to perform analysis, from which we obtained the peak position at 2055 cm^{-1}. For the SERS spectra recorded from aqueous suspensions of the 2,6-DMPI-functionalized Ag–Ir nanocubes prepared with 0.1 mL of Na_3IrCl_6 solution, we used three Gaussian–Lorentzian peaks with their positions fixed at 2169, 2117, and 2055 cm^{-1} to perform the curve fitting.

Instrumentation and characterization

We used Eppendorf 5430 centrifuge to collect and wash all solid samples. We used a Cary 50 spectrometer (Agilent Technologies, Santa Clara, CA) to record UV-vis spectra. We analyzed the Ir and Ag contents using an inductively-coupled plasma mass spectrometer (ICP-MS, NexION 300Q, PerkinElmer, Waltham, MA). We recorded TEM images on a HT7700 microscope (Hitachi, Tokyo, Japan) operated at 120 kV. We performed the high-angle annular dark field scanning electron microscopy (HAADF-STEM) imaging and energy-dispersive spectroscopy (EDS) mapping on a Hitachi HD2700C STEM operated at 200 kV and equipped with a probe aberration corrector.

Results and discussion

We followed the published protocol to synthesize Ag nanocubes with an average edge length of 38.7 ± 2.6 nm (Fig. S1†).[39] Firstly, we evaluated the shape stability of the as-prepared Ag nanocubes by re-dispersing them in a PVP/EG solution and heating in air to 110 °C, followed by the collection of samples from the suspension at different time points for characterization by UV-vis spectroscopy and transmission electron microscopy (TEM). Fig. S2A† shows UV-vis spectra recorded from the suspensions of the Ag nanocubes in a PVP/EG solution before and after the thermal treatment. It was found that the major LSPR peak of the Ag nanocubes located at 448 nm was blue-shifted to 434, 425, and 415 nm at t = 5, 10, and 30 min, respectively, together with a decrease in peak intensity. We also noticed that the two shoulder peaks located at 390 and 352 nm, with their origins being associated with the sharp corners and edges of a nanocube, became weaker in intensity.[40] Fig. S2B–D,† shows TEM images of the corresponding particles at the three time points, indicating the transformation of Ag nanocubes to nanospheres. Altogether, these results confirm that the edges and corners of the Ag nanocubes are more susceptible to oxidative etching of Ag atoms by the O_2 dissolved in the mixture owing to the higher surface energies of the {110} and {111} facets than that of the {100} facets. Although these dissolved Ag^+ ions could be reduced to Ag atoms by EG for their re-deposition on the nanoparticles, we suspect that the rate of oxidative etching was faster than that of reduction/deposition, contributing to the transformation from cubes to spheres, a shape more favorable in terms of thermodynamics.

We then demonstrated that the shape transformation could be impeded by depositing a small amount of Ir on the edges and corners of the Ag nanocubes for the generation Ag–Ir core-frame nanocubes. In a typical process, we dispersed Ag nanocubes in a mixture of EG and PVP at 110 °C, immediately followed by the titration of a Na_3IrCl_6/EG solution (see details in the Experimental section). Based on our previous work,[41–44] we argue that the added Na_3IrCl_6 could be reduced by EG (and possibly by Ag through a galvanic replacement mechanism) for the generation of Ir atoms, followed by their deposition onto the edges and then corners of the nanocubes. Fig. 1A shows a TEM image of the products obtained at a titration volume of 0.02 mL, which were essentially identical to the original Ag nanocubes in terms of shape and morphology. As the titration volume was increased to 0.05 mL, Fig. 1B shows that the corners of the nanocubes were sharpened, indicating the deposition of Ir onto the edges and then corners. When the titration volume was further increased to 0.1 mL, some of the nanocubes started to show slightly concaved side faces (Fig. 1C). The TEM images in Fig. 1D and E, show the formation of Ag–Ir nanocubes with more concaved side faces when the titration volume was increased to 0.2 and 0.4 mL, respectively. It is understandable that the continuous deposition of Ir atoms onto the edges and corners would eventually lead to the formation of concave nanocubes. It is also possible

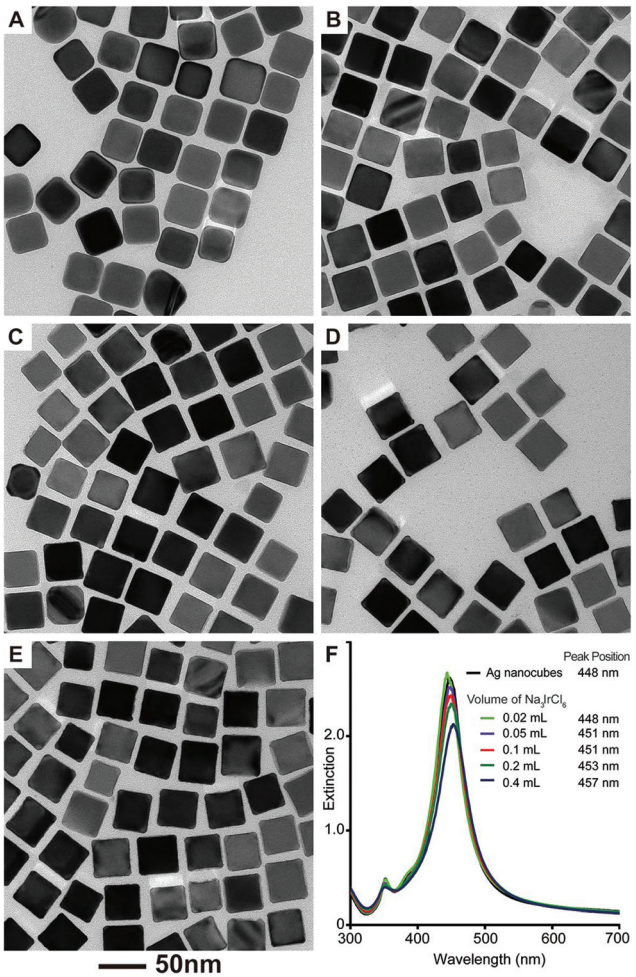

Fig. 1 TEM images of the Ag–Ir nanocubes that were prepared by reacting Ag nanocubes with different volumes of the Na_3IrCl_6/EG solution: (A) 0.02, (C) 0.05, (C) 0.1, (D) 0.2, and (E) 0.4 mL, respectively. (F) UV-vis spectra recorded from suspensions of the Ag nanocubes before and after reacting with different volumes of the Na_3IrCl_6 solution in a PVP/EG solution.

that galvanic replacement reaction could occur with an increase in the local concentration of Na_3IrCl_6. In turn, some of the Ag atoms on the side faces could be dissolved for the deposition of Ir on the other facets in an orthogonal manner, consistent with our previous findings.[42–44]

We also collected UV-vis spectra from the suspensions of the Ag nanocubes in a EG/PVP solution before and after they had reacted with different volumes of the Na_3IrCl_6/EG solution. At 0.02 mL, Fig. 1F shows that the major LSPR peak remained at 448 nm. However, as the titration volume was increased to 0.05, 0.1, 0.2, and 0.4 mL, this peak was red-shifted to 451, 451, 453 and 457 nm, respectively, supporting the gradual transformation into concave nanocubes. Additionally, we observed a slight decrease in the peak intensity, which could be attributed to the relatively weak interaction between Ir and light.[45] It is worth mentioning that, in all cases, we still resolved the weak peak at 352 nm, a signature inherent to the sharp corners of nanocubes, confirming the retention of cubic shape for the as-obtained Ag–Ir nanocrystals. Additionally, we noticed that the peak width of LSPR bands remained narrow, suggesting that the as-obtained nanocubes should exist in a solid rather than hollow structure. As a result, the Ir atoms should be mainly derived from the chemical reduction by EG rather than the galvanic replacement route.

We used inductively-coupled plasma mass spectrometry (ICP-MS) to confirm the deposition of Ir on the Ag nanocubes by measuring the Ag and Ir contents in both solid and supernatant products. Based on the data listed in Table S1,† the Ir to Ag atomic ratios of the Ag–Ir nanocubes prepared using 0.02, 0.05, 0.1, 0.2, and 0.4 mL, respectively, of the Na_3IrCl_6/EG solution were 1 : 444, 1 : 241, 1 : 165, 1 : 93, and 1 : 29. It is worth mentioning that the amount of Ag^+ ions in the supernatants for all samples were close to the detection limit. These results suggest that there was very limited dissolution of Ag through the galvanic replacement route during the deposition of Ir, consistent with the TEM and UV-vis results. It is also

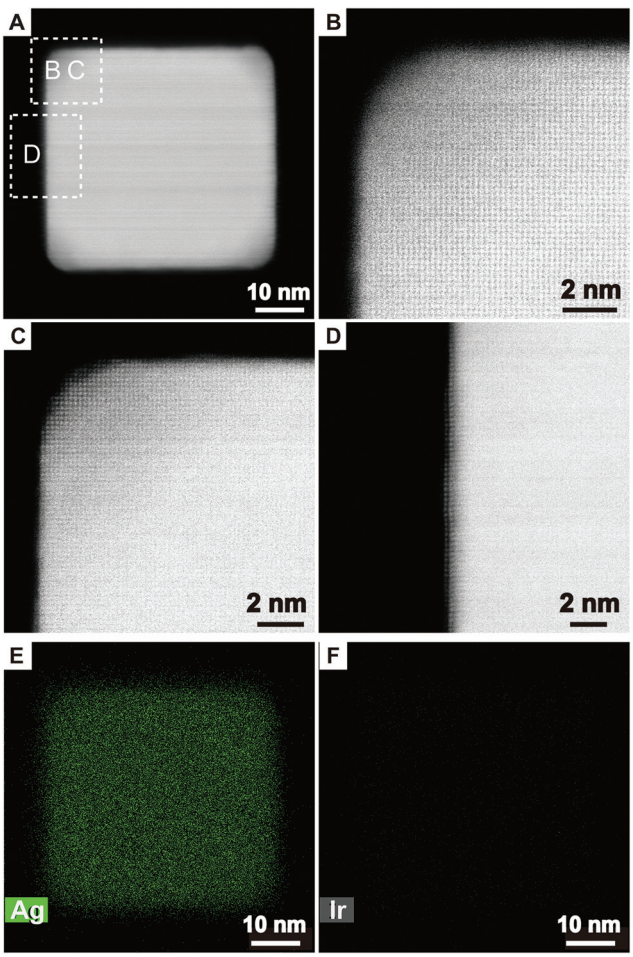

Fig. 2 (A–D) HAADF-STEM images of a Ag–Ir nanocube prepared by reacting Ag nanocubes with 0.1 mL of the Na_3IrCl_6/EG solution in a PVP/EG solution held at 110 °C. (E, F) EDS elemental mapping of the nanocube shown in (A).

This journal is © The Royal Society of Chemistry 2020

possible that the small amount of dissolved Ag^+ ions was reduced by EG for the generation of Ag atoms, followed by their deposition back onto the nanocubes.

In another attempt to verify the deposition and distribution of Ir on Ag nanocubes, we used high-angle annular dark-field scanning transmission electron microscopy (HAADF-STEM) to characterize the sample prepared with 0.1 mL of the Na_3IrCl_6/EG solution. Fig. 2A shows a HAADF-STEM image taken from a nanocube that was orientated along the [001] zone axis. Fig. 2B and C, gives two atomic-resolution HAADF-STEM images captured from one corner of the nanocube. By focusing the electron beam on the top of the nanocube, Fig. 2B shows the columns of Ag atoms located on the {100} facets, from which we could resolve some vague features of possible Ir atoms at the edges. Fig. 2C and D, shows some atoms located at the corners and edges of the nanocube after we refocused the electron beam away from the top to the bottom of the nanocube. In this case, we could no longer identify the columns of the Ag atoms. As such, those atoms located on the edges suggest the presence of Ir. We also made an attempt to collect energy-dispersive spectroscopy (EDS) mapping of the Ag and Ir atoms. As shown in Fig. 2E and F, we were able to detect the signals from Ag, but not from Ir, primarily because of the very small amount of Ir deposited on the Ag nanocubes.

We investigated the shape stability of the as-obtained Ag–Ir nanocubes by following the same protocol used for the original Ag nanocubes. For the Ag–Ir nanocubes prepared with 0.02 mL of the Na_3IrCl_6/EG solution, Fig. 3A shows the UV-vis spectra of the sample before and after the thermal treatment. We noticed that the major LSPR peak located at 447 nm was blue-shifted to 442, 438, and 430 nm at t = 5, 10, and 30 min, respectively. It is worth mentioning that this peak of Ag–Ir nanocubes was continuously decreased up to 10 min, indicating the dissolution of Ag atoms through oxidative etching. However, we observed an increase in the peak intensity by 30 min, suggesting that some dissolved Ag^+ ions in the reaction solution could be reduced by EG to newly formed Ag atoms for their redeposition on the nanoparticles. Fig. 3B–D, shows TEM images of the resultant nanoparticles at these three time points, from which we observed the formation of

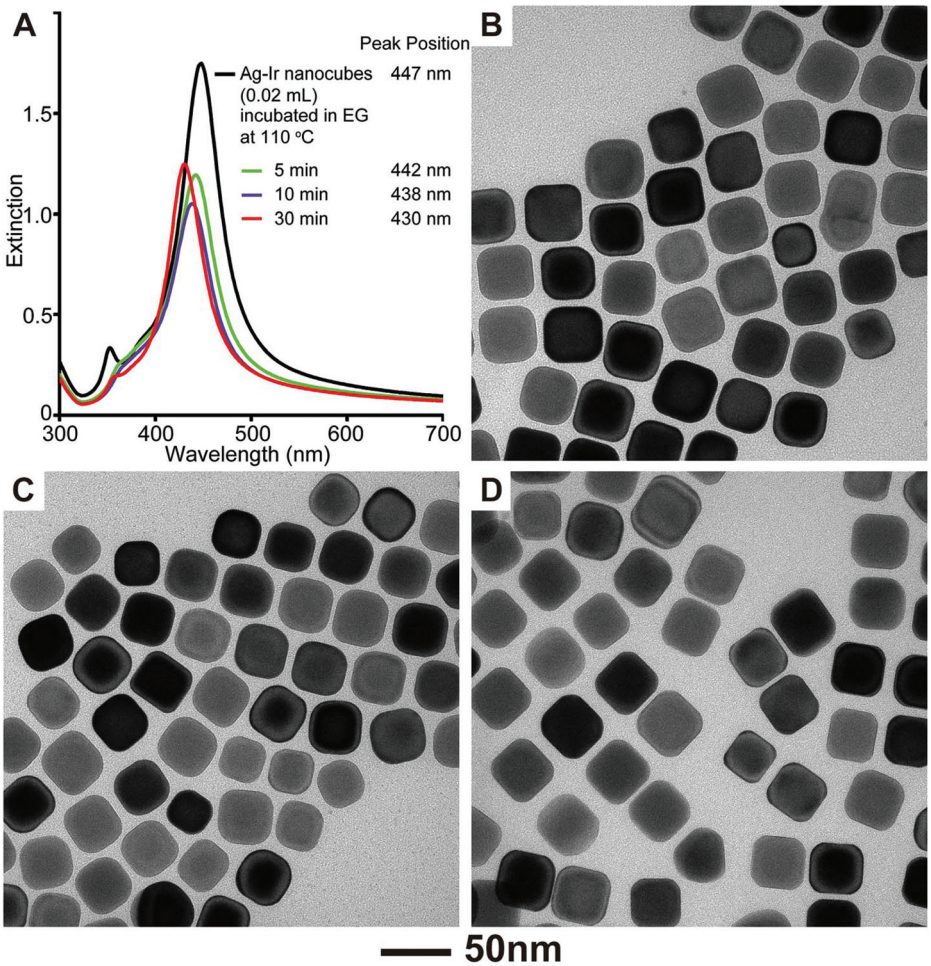

Fig. 3 (A) UV–vis spectra recorded from suspensions of the Ag–Ir nanocubes before and after they had been incubated in a PVP/EG solution at 110 °C for different periods of time. These Ag–Ir nanocubes were prepared by reacting the Ag nanocubes with 0.02 mL of the Na_3IrCl_6/EG solution. (C–D) TEM images of the resultant nanoparticles after thermal treatment for (B) 5, (C) 10, and (D) 30 min, respectively.

Ag–Ir nanocubes with truncation at all corners. These results suggest that the Ir atoms were mainly deposited on the edges of Ag nanocubes, leading to the truncation at corners due to the oxidation of Ag atoms by the O_2 dissolved in the mixture. When the volume of the Na_3IrCl_6/EG solution was increased to 0.05 mL, Fig. S3A† shows that the LSPR peak of the as-obtained Ag–Ir nanocubes was slightly shifted from 451 to 454, 455, and 454 nm at t = 5, 10, and 30 min, respectively. Fig. S3B–D,† provides TEM images of the resultant nanoparticles, from which we could identify truncations only at a limited number of corners as marked by circles. When the volume of the Na_3IrCl_6/EG solution was further increased to 0.1 mL, Fig. 4A shows that the LSPR peak located at 452 nm remained essentially the same before and after the thermal treatment up to t = 30 min. The TEM images in Fig. 4B–D, confirm that the cubic shape was well-preserved for all these three samples.

Because the deposition of Ir atoms on Ag nanocubes could protect Ag atoms from oxidation, we rely on the morphology of the Ag–Ir nanocubes before and after shape stability test to decipher the deposition pathway for the Ir atoms. As illustrated in Fig. 5, we can maneuver the number of Ir atoms being deposited on the different facets of Ag nanocubes by simply controlling the titration volume of the Na_3IrCl_6/EG solution. For example, at a titration volume of 0.02 mL, we argue that the Ir atoms derived from the reduction of Na_3IrCl_6 would be mainly deposited on all edges of the Ag nanocubes. At 0.05 mL, the deposition of Ir atoms was extended from edges to some corners of the nanocubes. At 0.1 mL, all edges and corners of the nanocubes were covered by Ir atoms. To validate our proposed mechanism, we performed back-of-the-envelope calculations to estimate the Ir coverage on the edges or both edges and corners of a Ag nanocube with the physical dimensions defined in Fig. S4 (see Appendices 1–3† for details). It is worth mentioning that we used the TEM images of Ag nanocubes (see Fig. S1†) to define the edge length and the truncation of a corner for a nanocube shown in Fig. S4.† Based on our prior publication for the fabrication of Ag–Pd nanoframes with ridges as thin as 1.7 nm by depositing Pd on the edges of Ag nanocubes,[46] we assumed that the width of an edge was

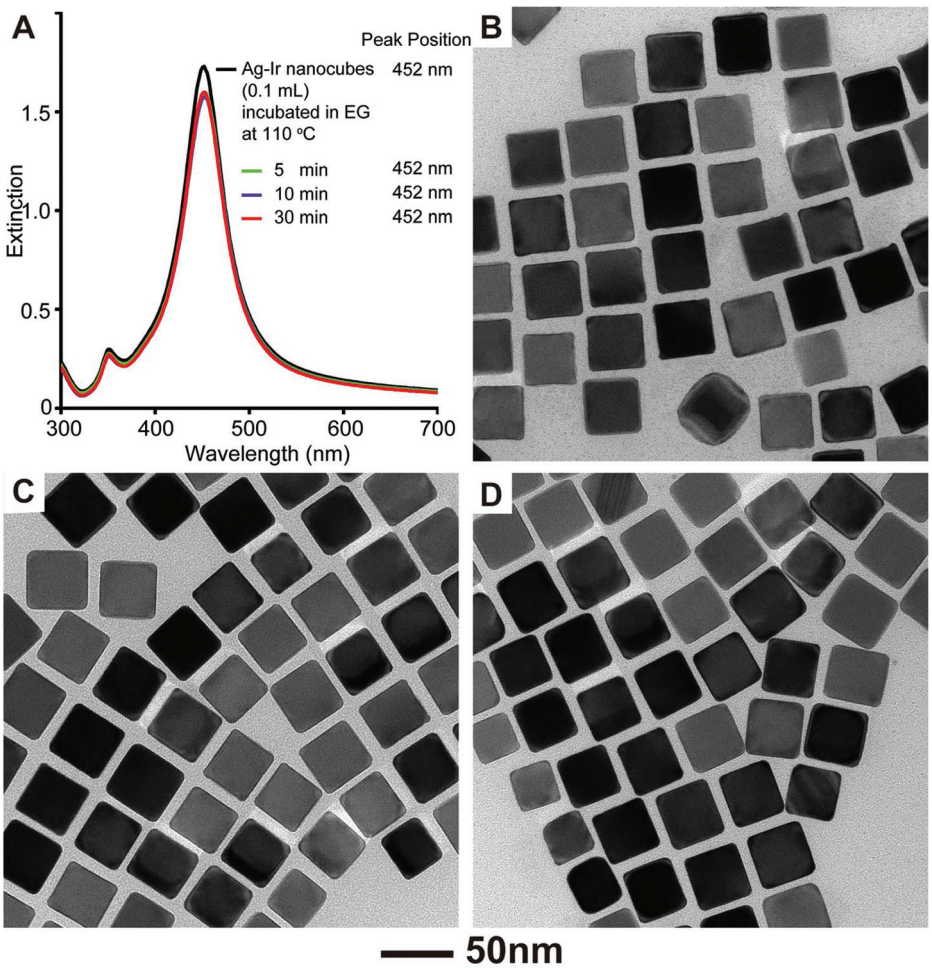

Fig. 4 (A) UV–vis spectra recorded from suspensions of the Ag–Ir nanocubes before and after they had been incubated in a PVP/EG solution at 110 °C for different periods of time. These Ag–Ir nanocubes were prepared by reacting the Ag nanocubes with 0.1 mL of the Na_3IrCl_6/EG solution. (C–D) TEM images of the resultant nanoparticles after the thermal treatment for (B) 5, (C) 10, and (D) 30 min, respectively.

This journal is © The Royal Society of Chemistry 2020

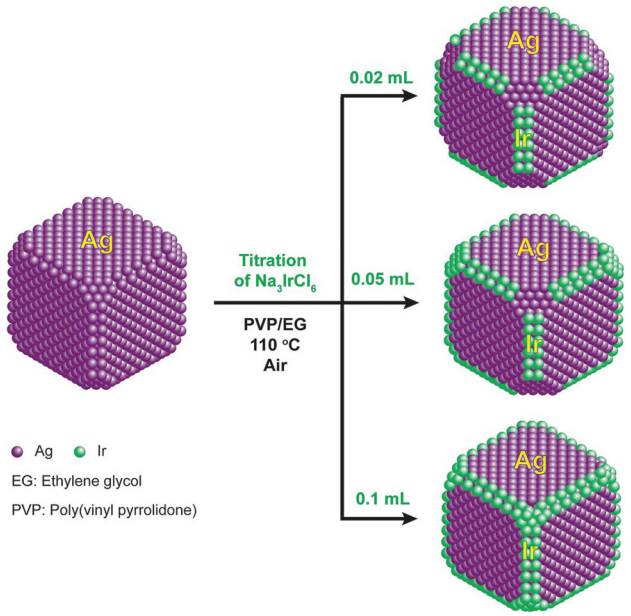

Fig. 5 Schematic illustration showing the increased deposition of Ir atoms onto the edges and corners of a Ag nanocube as the titration volume of the Na_3IrCl_6 solution is increased.

1.5 nm. We used the mass of Ag and Ir contents of the Ag–Ir nanocubes shown in Table S1† to calculate the coverage of Ir atoms on the surface of all edges or both the edges and corners of Ag nanocubes at titration volumes of 0.02, 0.05, and 0.1 mL, respectively. Table 1 summarizes the results. At a titration volume of 0.02 mL, the Ir atoms could cover 59.4% of all the edges (or 34.6% of both edges and corners) on a single nanocube, which supports the transformation of the corresponding Ag–Ir nanocubes into truncated nanocubes as shown in Fig. 3. At 0.05 mL, the coverage of Ir atoms increased to 64.9% of both edges and corners (or 111.6% of all edges) of a nanocube. This result suggests the deposition of Ir atoms on all edges and some corners of a nanocube, consistent with the shape stability results shown in Fig. S3.† At 0.1 mL, the Ir atoms could cover 99.5% of both edges and corners (or 170.0% of all edges) of a nanocube, making it possible to preserve the shape of the Ag–Ir nanocubes as demonstrated in Fig. 4. Altogether, our calculation results support the proposed mechanism illustrated in Fig. 5.

We evaluated the plasmonic properties of the Ag–Ir nanocubes by benchmarking against the original Ag nanocubes. As demonstrated in Fig. 1F, the as-prepared Ag–Ir nanocubes exhibited LSPR properties essentially identical to those of the original Ag nanocubes. We also assessed the SERS activity of these bimetallic nanocubes by using 2,6-dimethylphenyl isocyanide (2,6-DMPI) as a unique probe to characterize the outermost surface of nanocubes. Based on our previous studies,[42,43,47,48] we argue that the lone pair of electrons would bind to Ag and Ir through σ-donation and π-back-donation, respectively, making it possible to characterize the Ag and Ir atoms by following the NC stretching (ν_{NC}) peak. It is worth mentioning that we noticed the aggregation of nanoparticles after we followed the procedure described in the Experimental section for the SERS measurements in water. Fig. S5† shows the UV-vis spectra of 2,6-DMPI-functionalized Ag and Ag–Ir nanocubes before SERS measurements, from which we observed the appearance of a shoulder peak in the range of 500 to 700 nm for each sample. We suspect that this band is attributed to the dipolar mode of these assembled particles due to the coupling between the dipole mode of each nanocube.[49] In this case, the broad peak is in resonance with the laser excitation wavelength at 532 nm. Although the SERS signal arises mainly from the SERS hotspots located between nanocubes, we believe that SERS spectra could provide the fingerprinting spectroscopy of isocyanide probe with its binding to Ag and Ir atoms on the edges of Ag nanocubes distinctively. Fig. 6 shows the SERS spectra of 2,6-DMPI adsorbed onto the Ag nanocubes before and after they had reacted with different volumes of the Na_3IrCl_6/EG solution, after the background had been subtracted. The raw SERS data is given in Fig. S6.† Before titration, we observed the peak located at 2169 cm^{-1} with its assignment to the NC stretching ($\nu_{NC(Ag)}$) band of 2,6-DMPI, together with other bands of 2,6-DMPI.[42,43,50] In fact, we fitted the $\nu_{NC(Ag)}$ band using one Gaussian–Lorentzian peak (Fig. S7A†). At a titration volume of 0.02 mL, we noticed the appearance of a broader and a weaker band with which we used two Gaussian–Lorentzian peaks, with their assignment to the $\nu_{NC(Ag)}$ band at 2169 cm^{-1} and the $\nu_{NC(Ir)}$ band at 2117 cm^{-1}, respectively, to simulate this band (Fig. S7B†). Our result suggests that the outermost surface consists of both Ag and Ir atoms, making the edges of nanocubes not fully covered by Ir atoms yet. As such, these as-obtained Ag–Ir nanocubes were converted into truncated ones after thermal treatment (see Fig. 3B–D). At 0.05 mL, we used the $\nu_{NC(Ag)}$ band at 2169 cm^{-1}, the $\nu_{NC(Ir)}$ band at 2117 cm^{-1}, and another $\nu_{NC(Ir)}$ band at 2055 cm^{-1} to fit the SERS peak (Fig. S7C†), from which we noticed that the contribution from the $\nu_{NC(Ag)}$ band significantly decreased. Based on our previous study on the isocyanide binding on Pd atoms,[46] we tentatively assigned the $\nu_{NC(Ir)}$ band at 2117 and 2055 cm^{-1} to atop and hollow/bridge configuration upon binding of isocyanide to Ir atoms. Likely,

Table 1 The calculated coverage of Ir monolayer on the edges and corners of a Ag nanocube

	Ir monolayer coverage on all the edges of a nanocube	Ir monolayer coverage on all the edges and corners of a nanocube
Sample 1 (0.02 mL Na_3IrCl_6)	59.4%	34.6%
Sample 2 (0.05 mL Na_3IrCl_6)	111.6%	64.9%
Sample 3 (0.1 mL Na_3IrCl_6)	170.0%	99.5%

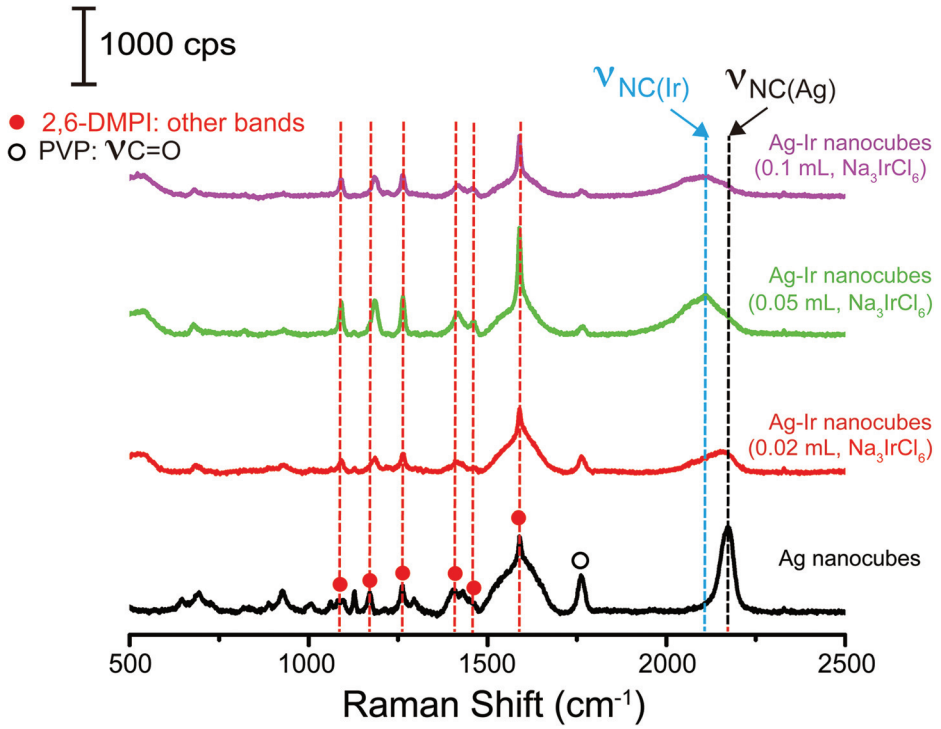

Fig. 6 SERS spectra recorded from aqueous suspensions of the 2,6-DMPI-functionalized Ag–Ir nanocubes under the excitation of a 532 nm laser. The background has been subtracted from the as-recorded spectra. The Ag–Ir nanocubes were prepared by reacting the Ag nanocubes with different volumes of the Na_3IrCl_6/EG solution, as marked on each spectrum.

the edges of the Ag–Ir nanocubes were fully covered by Ir atoms, and as a result, the edges could survive the shape stability test (see Fig. S3B–D†). As the volume of the Na_3IrCl_6 solution was further increased to 0.1 mL, we could fit the SERS peak using the $\nu_{NC(Ag)}$ band at 2169 cm^{-1} and two $\nu_{NC(Ir)}$ bands at 2117 and 2055 cm^{-1} (Fig. S7D†). Again, the contribution from the $\nu_{NC(Ag)}$ band was rather limited. It is also worth mentioning that the SERS signal was deteriorated due to the weak coupling between the conduction electrons of Ir and visible light.[13,51] These results indicate that the deposited Ir atoms were able to cover the entire surface of the edges and corners, in agreement with our previous observation on the excellent shape stability of Ag–Ir nanocubes (see Fig. 4B–D). We also evaluated the other bands of 1,4-DMPI located from 1000–1600 cm^{-1}.[50] Among these peaks, we observed the continuous blueshift of the C–H in plane bending mode from 1170 to 1186 cm^{-1} as the Ag–Ir ratio increases while the other bands remained essentially the same. Collectively, our results demonstrate that these Ag–Ir nanocubes embrace both LSPR and SERS properties almost identical to those of the original Ag nanocubes.

Conclusions

We have demonstrated that the deposition of a corrosion-resistant metal such as Ir on the edges and corners of Ag nanocubes could retard the oxidation of Ag atoms from these sites and thereby enhance their shape stability. The synthesis simply involves the titration of a Na_3IrCl_6/EG solution into a suspension of Ag nanocubes in a PVP/EG solution held at 110 °C. By controlling the titration volume of the Na_3IrCl_6/EG solution, we demonstrate an exquisite control over the coverage of the Ir atoms on the edges and corners for the generation of Ag–Ir core-frame nanocubes. Our stability test establishes that the edges and corners of the Ag nanocubes only need to be covered by small amount of Ir atoms in order to retain their cubic shape when aged in a PVP/EG solution at 110 °C. We believe that this strategy can be extended to enhance the stability of Ag nanocubes with different sizes. Significantly, the Ag–Ir nanocubes exhibit LSPR and SERS properties largely the same as those of the original Ag nanocubes. We believe that a combination of excellent plasmonic properties and shape stability will open the door to a variety of new applications.

Conflicts of interest

There are no conflicts to declare.

Acknowledgements

We acknowledge the support from the National Science Foundation (CHE-1708300) and ACS Petroleum Research Fund (PRF# 59664-ND10). We acknowledge the use of the character-

 This journal is © The Royal Society of Chemistry 2020

ization facility at the Institute of Electronics and Nanotechnology (IEN) at GT. We acknowledge Ruhui Chen in support of quantitative measurements of Ir and Ag contents by using ICP-MS. P. W. acknowledges the financial support from China Scholarship Council.

References

1 Z. Fan and H. Zhang, *Acc. Chem. Res.*, 2016, **49**, 2841–2850.
2 S. A. Maier, P. G. Kik, H. A. Atwater, S. Meltzer, E. Harel, B. E. Koel and A. A. G. Requicha, *Nat. Mater.*, 2003, **2**, 229–232.
3 S. Linic, P. Christopher and D. B. Ingram, *Nat. Mater.*, 2011, **10**, 911–921.
4 P. K. Jain, X. Huang, I. H. El-Sayed and M. A. El-Sayed, *Acc. Chem. Res.*, 2008, **41**, 1578–1586.
5 J. N. Anker, W. P. Hall, O. Lyandres, N. C. Shah, J. Zhao and R. P. Van Duyne, *Nat. Mater.*, 2008, **7**, 442–453.
6 Y. Xia, Y. Xiong, B. Lim and S. E. Skabalak, *Angew. Chem., Int. Ed.*, 2009, **48**, 60–103.
7 K. A. Willets and R. P. Van Duyne, *Annu. Rev. Phys. Chem.*, 2007, **58**, 267–297.
8 Z. Peng and H. Yang, *Nano Today*, 2009, **4**, 143–164.
9 S. Mostafa, F. Behafarid, J. R. Croy, L. K. Ono, L. Li, J. C. Yang, A. I. Frenkel and B. R. Cuenya, *J. Am. Chem. Soc.*, 2010, **132**, 15714–15719.
10 A.-X. Yin, X.-Q. Min, Y.-W. Zhang and C.-H. Yan, *J. Am. Chem. Soc.*, 2011, **133**, 3816–3819.
11 A. Tao, P. Sinsermsuksakul and P. Yang, *Angew. Chem., Int. Ed.*, 2006, **45**, 4597–4601.
12 B. J. Wiley, S. H. Im, Z.-Y. Li, J. McLellan, A. Siekkinen and Y. Xia, *J. Phys. Chem. B*, 2006, **110**, 15666–15675.
13 P. L. Stiles, J. A. Dieringer, N. C. Shah and R. P. Van Duyne, *Annu. Rev. Phys. Chem.*, 2008, **1**, 601–626.
14 J. Reguera, J. Langer, D. Jiménez de Aberasturi and L. M. Liz-Marzán, *Chem. Soc. Rev.*, 2017, **46**, 3866–3885.
15 R. Narayanan and M. A. El-Sayed, *Nano Lett.*, 2004, **4**, 1343–1348.
16 Z. Quan, Y. Wang and J. Fang, *Acc. Chem. Res.*, 2013, **46**, 191–202.
17 K. Zhou and Y. Li, *Angew. Chem., Int. Ed.*, 2012, **51**, 602–613.
18 P. Christopher and S. Linic, *ChemCatChem*, 2010, **2**, 78–83.
19 A. R. Tao, S. Habas and P. Yang, *Small*, 2008, **4**, 310–325.
20 L. Ruan, C.-Y. Chiu, Y. Li and Y. Huang, *Nano Lett.*, 2011, **11**, 3040–3046.
21 G. Collins, M. Schmidt, C. O'Dwyer, G. McGlacken and J. D. Holmes, *ACS Catal.*, 2014, **4**, 3105–3111.
22 Y. Xia, X. Xia and H.-C. Peng, *J. Am. Chem. Soc.*, 2015, **134**, 7947–7966.
23 X. Qi and K. A. Fichthorn, *Nanoscale*, 2017, **9**, 15635–15642.
24 Y. Sun and Y. Xia, *Science*, 2002, **298**, 2176–2179.
25 Z. L. Wang, *J. Phys. Chem. B*, 2000, **104**, 1153–1175.
26 X. Xia, J. Zeng, L. K. Oetjen, Q. Li and Y. Xia, *J. Am. Chem. Soc.*, 2012, **134**, 1793–1801.
27 Z. Chen, J. W. Chang, C. Balasanthiran, S. T. Milner and R. M. Rioux, *J. Am. Chem. Soc.*, 2019, **141**, 4328–4337.
28 Q. Zhang, I. Lee, J. Ge, F. Zaera and Y. Yin, *Adv. Funct. Mater.*, 2010, **20**, 2201–2214.
29 Q. Zhang, J. Ge, T. Pham, J. Goebl, Y. Hu, Z. Lu and Y. Yin, *Angew. Chem., Int. Ed.*, 2009, **48**, 3516–3519.
30 J. Feng, C. Gao and Y. Yin, *Nanoscale*, 2018, **10**, 20492–20504.
31 J. M. McLellan, A. Siekkinen, J. Chen and Y. Xia, *Chem. Phys. Lett.*, 2006, **427**, 122–126.
32 P. Christopher and S. Linic, *ChemCatChem*, 2010, **2**, 78–83.
33 Z. L. Wang, T. S. Ahmad and M. A. El-Sayed, *Surf. Sci.*, 1997, **380**, 302–310.
34 M. J. Mulvihill, X. Y. Ling, J. Henzie and P. Yang, *J. Am. Chem. Soc.*, 2010, **132**, 268–274.
35 Z. Wang, G. Yang, Z. Zhang, M. Jin and Y. Yin, *ACS Nano*, 2016, **10**, 4559–4564.
36 M. J. N. Pourbaix, J. V. Muylder and N. D. Zoubov, *Platinum Metals Rev.*, 1959, **3**, 100–106.
37 M. J. Cawkwell, D. Nguyen-Manh, C. Woodward, D. G. Pettifor and V. Vitek, *Science*, 2005, **309**, 1059–1062.
38 H. Guo, H. Li, K. Jarvis, H. Wan, P. Kunal, S. G. Dunning, Y. Liu, G. Henkelman and S. M. Humphrey, *ACS Catal.*, 2018, **8**, 11386–11397.
39 Q. Zhang, W. Li, L. Wen, J. Chen and Y. Xia, *Chem. – Eur. J.*, 2010, **16**, 10234–10239.
40 F. Lu, Y. Tian, M. Liu, D. Su, H. Zhang, A. O. Govorov and G. Oleg, *Nano Lett.*, 2013, **13**, 3145–3151.
41 L. Zhang, Y. Zhang, J. Ahn, X. Wang and D. Qin, *Chem. Mater.*, 2019, **31**, 1057–1065.
42 Y. Zhang, J. Ahn, J. Liu and D. Qin, *Chem. Mater.*, 2018, **30**, 2151–2159.
43 Y. Zhang, J. Liu, J. Ahn, T. Xiao, Z.-Y. Li and D. Qin, *ACS Nano*, 2017, **11**, 5080–5086.
44 J. Ahn, D. Wang, Y. Ding, J. Zhang and D. Qin, *ACS Nano*, 2018, **12**, 298–307.
45 G. Kang, A. Matikainen, P. Stenberg, E. Färm, P. Li, M. Ritala, P. Vahimaa, S. Honkanen and X. Tan, *ACS Appl. Mater. Interfaces*, 2015, **7**, 11452–11459.
46 J. Li, X. Sun and D. Qin, *ChemNanoMat*, 2016, **2**, 494–499.
47 Y. Wu and D. Qin, *J. Am. Chem. Soc.*, 2018, **140**, 8340–8349.
48 Z. Luo, J. Ahn and D. Qin, *Nanoscale*, 2019, **11**, 6710–6718.
49 N. Hooshmanda and A. E. Mostafa, *Proc. Natl. Acad. Sci. U. S. A.*, 2019, **116**, 19299–19304.
50 K. Kim, K. L. Kim, J.-Y. Choi, L. B. Lee and K. S. Shin, *J. Phys. Chem. C*, 2010, **114**, 3448–3453.
51 K. Chakrapani and S. Sampath, *Chem. Commun.*, 2014, **50**, 3061–3063.

This journal is © The Royal Society of Chemistry 2020